

*Large-scale length and time scales for use  
with stochastic convective  
parameterization*

Article

Published Version

Plant, R. S. and Keane, R. J. (2011) Large-scale length and time scales for use with stochastic convective parameterization. Quarterly Journal of the Royal Meteorological Society, 138 (666). pp. 1150-1164. ISSN 1477-870X doi: <https://doi.org/10.1002/qj.992> Available at <http://centaur.reading.ac.uk/24795/>

It is advisable to refer to the publisher's version if you intend to cite from the work. See [Guidance on citing](#).

To link to this article DOI: <http://dx.doi.org/10.1002/qj.992>

Publisher: Royal Meteorological Society

All outputs in CentAUR are protected by Intellectual Property Rights law, including copyright law. Copyright and IPR is retained by the creators or other copyright holders. Terms and conditions for use of this material are defined in

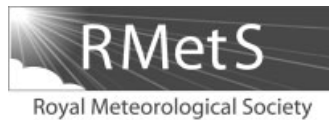
the [End User Agreement](#).

[www.reading.ac.uk/centaur](http://www.reading.ac.uk/centaur)

## **CentAUR**

Central Archive at the University of Reading

Reading's research outputs online



# Large-scale length and time-scales for use with stochastic convective parametrization

R. J. Keane\* and R. S. Plant

*Department of Meteorology, University of Reading, UK*

\*Correspondence to: R. J. Keane, Meteorologisches Institut, Ludwig-Maximilians-Universität München, Fakultät für Physik, Theresienstr. 37, 80333 München, Germany. E-mail: richard.keane@lmu.de

Many numerical models for weather prediction and climate studies are run at resolutions that are too coarse to resolve convection explicitly, but too fine to justify the local equilibrium assumed by conventional convective parametrizations. The Plant–Craig (PC) stochastic convective parametrization scheme, developed in this paper, solves this problem by removing the assumption that a given grid-scale situation must always produce the same sub-grid-scale convective response. Instead, for each time step and grid point, one of the many possible convective responses consistent with the large-scale situation is randomly selected. The scheme requires as input the large-scale state as opposed to the instantaneous grid-scale state, but must nonetheless be able to account for genuine variations in the large-scale situation. Here we investigate the behaviour of the PC scheme in three-dimensional simulations of radiative–convective equilibrium, demonstrating in particular that the necessary space–time averaging required to produce a good representation of the input large-scale state is not in conflict with the requirement to capture large-scale variations. The resulting equilibrium profiles agree well with those obtained from established deterministic schemes, and with corresponding cloud-resolving model simulations. Unlike the conventional schemes, the statistics for mass flux and rainfall variability from the PC scheme also agree well with relevant theory and vary appropriately with spatial scale. The scheme is further shown to adapt automatically to changes in grid length and in forcing strength. Copyright © 2011 Royal Meteorological Society

*Key Words:* stochastic parametrization; convection; ensemble averaging

*Received 5 May 2011; Revised 13 October 2011; Accepted 13 November 2011; Published online in Wiley Online Library 19 December 2011*

*Citation:* Keane RJ, Plant RS. 2012. Large-scale length and time-scales for use with stochastic convective parametrization. *Q. J. R. Meteorol. Soc.* **138**: 1150–1164. DOI:10.1002/qj.992

## 1. Introduction

Forecast errors in numerical simulations of the atmosphere arise from uncertainties in the initial and boundary conditions, in the external forcings, and also in the model formulation itself. Structural model uncertainties primarily relate to unresolved or poorly resolved physical processes that must be parametrized. These uncertainties are important because small-scale fluctuations can interact with grid-scale dynamics, leading to upscale growth of errors

(e.g. Zhang *et al.*, 2003). This contributes to the spreading of ensemble weather forecasts, and as a consequence the ensemble spreads produced by systems accounting for initial-condition uncertainty alone are often insufficient to cover the full range of possible flows (Buizza, 1997; Buizza *et al.*, 2005). The variability can be increased in such systems so that it is more representative of the real atmosphere, but only at the cost of carefully inflating the initial condition perturbations (e.g. Bowler *et al.*, 2008).

Over the last decade, various methods have been introduced in order to provide explicit representations of

some of the uncertainties arising from the parametrizations in numerical weather prediction (NWP) and general circulation models (GCMs). Although some of the methods are somewhat ad hoc, they are nonetheless beneficial and can provide more satisfactory treatments of model uncertainty than simple inflation of initial-condition perturbations. For example, Buizza *et al.* (1999) add a random perturbation to the tendencies obtained from the parametrization schemes. Other authors have included stochastic elements directly in a parametrization scheme itself. As examples, Bright and Mullen (2002) introduced a stochastic component to the trigger function of a convection scheme, Lin and Neelin (2003) added random perturbations to the convective available potential energy (CAPE) closure and, separately, to the vertical heating profile, and Shutts (2005) developed a stochastic kinetic energy backscatter scheme, where a fraction of the energy dissipated by the model grid truncation is reintroduced near the model grid scale. A good overview of current methods can be found in a recent book (Williams and Palmer, 2009).

The Plant and Craig (2008, hereinafter PC) stochastic convection parametrization scheme is designed to produce physically realistic convective variability and to adapt automatically to changes in the resolution of the parent model, down to grid lengths of the order of 10 km. For large grid lengths, where the variability is suitably low, the scheme should agree with results from conventional deterministic convection schemes. Plant and Craig (2008) demonstrated these features in some single-column radiative–convective equilibrium (RCE) experiments, while Ball and Plant (2008) demonstrated that for grid lengths of  $\sim 50$  km then the convective fluctuations it produces become of comparable importance to the variability produced by some of the generic methods in use for representing structural model uncertainty. Thus, the PC scheme would appear to be particularly well suited for use at grid lengths of  $\sim 10$ – $50$  km, and even on variable resolution grids. However, the experiments just cited used single-column models. The implementation of any stochastic parametrization within a full, three-dimensional atmospheric model raises important scientific issues about the spatial and temporal scales associated with the parametrization and their relationship to the scales of the numerical model. The present article will establish the extent to which the input profile to the scheme must be averaged in order to reproduce the correct convective variability and to adapt appropriately to model resolution.

The PC scheme is based on the statistical mechanics theory of Craig and Cohen (2006) for non-interacting clouds at equilibrium, and is supported by the results from cloud-resolving models (CRMs) in RCE (Cohen and Craig, 2006; Davoudi *et al.*, 2010). Conventional convective parametrizations are deterministic, so that the same sub-grid-scale convective response is always output for a given grid-scale input. However, CRMs clearly demonstrate that a wide range of convective states are consistent with a given grid-scale situation, for the grid sizes currently used in NWP and GCMs (Xu *et al.*, 1992; Cohen and Craig, 2006; Shutts and Palmer, 2007; Jones and Randall, 2011). The Craig and Cohen (2006) theory predicts analytical formulae for convective statistics which can be compared with the results produced by a convective parametrization. We will perform such tests at different grid lengths, in order to prove

that the PC scheme does indeed operate in a fully self-consistent way, independent of resolution. Results will also be compared with those of deterministic parametrization schemes, and with CRM results.

Three-dimensional RCE simulations are performed with a specified tropospheric cooling rate and parametrized convection over a uniform sea surface. The set-up is described in section 2, alongside key points from the theory against which the simulated convective variability is to be compared. The comparison itself is presented in section 3 and used to determine parameter settings and strategies for use of the PC scheme in three dimensions. The theory is extended in section 4 to study fluctuations in the rainfall rate, enabling the PC scheme to be compared directly to other convection schemes. Finally, section 5 discusses the implications of the results.

## 2. Methodology

### 2.1. Theory of convective variability

In order to make the present article self-contained, we provide here an overview of the theory for convective variability in equilibrium, and in the following subsection an overview of its implementation within the PC scheme.

An equilibrium condition supports an ensemble of possible states for the cumulus cloud field. Here, a ‘cloud’ is defined as an updraught (or updraught–downdraught pair) with mass flux due to a vertical velocity above some threshold. The possible cloud states are described by the mass fluxes  $m(z)$  for each of the variable number of clouds present. Following normal parametrization practice a description of the mass flux evolution over the lifetime of each cloud is not considered, and so the mass flux should be regarded as a lifetime-averaged value. Using statistical mechanics theory for non-interacting clouds, Craig and Cohen (2006) showed that the probability distribution function (PDF) of mass flux for the individual clouds is given by

$$p(m)dm = \frac{1}{\langle m \rangle} e^{-m/\langle m \rangle} dm, \quad (1)$$

where the angle brackets denote an ensemble average. The distribution has been verified in CRM experiments (Cohen and Craig, 2006; Davies, 2008; Davoudi *et al.*, 2010) and is robust for different heights and large-scale environments.

Following Plant and Craig (2008), for the experiments in this paper we take  $\langle m \rangle$  at the lifting condensation level (LCL) to be a constant,  $\langle m \rangle = 2 \times 10^7$  kg s<sup>-1</sup>. Various CRM studies (e.g. Robe and Emanuel, 1996; Shutts and Gray, 1999; Cohen, 2001; Parodi and Emanuel, 2009) have shown that the strength of the forcing seems to have only a weak effect on the mean mass flux of individual clouds: rather, a change in forcing is associated mainly with a change in the mean number of clouds  $\langle N \rangle$ . A recent CRM investigation by Davies and Jakob (2011, pers. comm.) shows that the vertical profile of  $\langle m \rangle$  may depend on some rather subtle changes to the character of the forcing, but nonetheless it finds very little sensitivity in  $\langle m \rangle$  in the lower atmosphere. In the observational literature, differences in typical convective core strengths between different regions and over different surface types have been identified and discussed (e.g. LeMone and Zipser, 1980; Lucas *et al.*, 1994; May and Rajopadhyaya, 1999) but we are not aware of studies

indicating systematic variations of  $\langle m \rangle$  at the LCL that might usefully be incorporated into the parametrization.

The total mass flux will be denoted  $M$ , and its ensemble-mean value  $\langle M \rangle$  can be taken to be known because of the equilibrium assumption. Given this constraint, a PDF for the total mass flux can be calculated, following Craig and Cohen (2006), as

$$p(M) = \delta(M) e^{-\frac{\langle M \rangle}{\langle m \rangle}} + \frac{1}{\langle m \rangle} \sqrt{\frac{\langle M \rangle}{M}} e^{-\frac{M + \langle M \rangle}{\langle m \rangle}} I_1 \left( \frac{2}{\langle m \rangle} \sqrt{M \langle M \rangle} \right), \quad (2)$$

where  $I_1$  is the modified Bessel function of order 1. This distribution has also been verified in CRM experiments (Cohen and Craig, 2006; Davoudi *et al.*, 2010). In section 3 we will investigate whether it can be reproduced in three-dimensional RCE experiments with parametrized convection. It will be convenient there to summarize some of the results by comparing with the theoretical prediction for the variance of  $M$ , which is

$$\langle (M - \langle M \rangle)^2 \rangle = 2 \langle M \rangle \langle m \rangle. \quad (3)$$

## 2.2. Implementation as a stochastic parametrization

The PC scheme is based on the theory outlined in the previous subsection. Full details are available in Plant and Craig (2008) but we present here a summary of the main aspects that are relevant for the present study. The first step is that the ensemble-mean mass flux at the LCL,  $\langle M \rangle$ , must be computed from the closure conditions of the scheme. Postponing our discussion of this crucial issue for the moment, the next step is then to determine the mass fluxes of individual clouds that constitute a possible, particular realization of the convective state at the grid box and time in question.

To model each individual cloud, the plume model from the Kain–Fritsch parametrization (Kain and Fritsch, 1990; Kain, 2004, hereinafter KF) is used, adapted to handle a spectrum of cloud types as described in Plant and Craig (2008). The KF scheme entraining/detraining plume model uses a buoyancy sorting approach in which it considers various possible mixtures of updraught and environmental air and retains each mixture in the updraught or else detrains it to the environment according to whether the mixture is positively or negatively buoyant, respectively. The calculations require a maximum entrainment rate to be specified, which is taken to be inversely proportional to the updraught radius:

$$\epsilon = \frac{-0.03 \delta p}{r}, \quad (4)$$

where  $\epsilon$  is the maximum entrainment per unit of mass flux within a pressure interval  $\delta p$  and for an updraught radius of  $r$ . Full details are given in Kain and Fritsch (1990). In the PC scheme the updraught radius is related to cloud mass flux by assuming that close to the LCL the mass flux varies only with the horizontal area of the cloud,

$$m = \frac{\langle m \rangle}{\langle r^2 \rangle} r^2. \quad (5)$$

Using the above equation, the PDF of cloud mass fluxes in Eq. (1) can be transformed into a PDF  $p(r)$  of cloud radii (and, therefore, of entrainment rates):

$$p(r) dr = \frac{2r}{\langle r^2 \rangle} \exp \left( \frac{-r^2}{\langle r^2 \rangle} \right) dr. \quad (6)$$

This equation is used to determine how many clouds to initiate, and of what sizes, within a given grid box in the PC scheme. Because it applies to a single cloud, it is rescaled to account for the fact that a number of clouds can be present in a grid box, by multiplying by  $\langle N \rangle$ . This is obtained from the large-scale state by using  $\langle N \rangle = \langle M \rangle / \langle m \rangle$ . It is also multiplied by a factor  $dt/T_L$  to allow for the finite lifetime  $T_L$  of the clouds ( $dt$  is the model time step): proportionally fewer clouds are initiated to allow for the fact that they persist for multiple time steps, as in the KF scheme. The initiation probability, then, within a model time step for a plume with radius  $r$  to  $r + dr$  is as follows:

$$\frac{\langle M \rangle}{\langle m \rangle} p(r) dr \frac{dt}{T_L} = \frac{\langle M \rangle}{\langle m \rangle} \frac{2r}{\langle r^2 \rangle} \exp \left( \frac{-r^2}{\langle r^2 \rangle} \right) dr \frac{dt}{T_L}. \quad (7)$$

Clouds are initiated at random from that PDF by binning the cloud spectrum into finite bins of width  $dr$ . The bin width is chosen so that the chance of two clouds occurring in the same bin is suitably negligible. For each bin, a random number uniformly distributed between zero and unity is generated and compared to the initiation probability. If the random number is lower then a cloud is initiated of that size. This paper follows Plant and Craig (2008) by setting  $T_L = 45$  min, a constant. It is easy to check that the normalization of Eq. (7) is such that the average number of clouds present is  $\langle N \rangle = \langle M \rangle / \langle m \rangle$ .

The persistence of clouds across multiple time steps introduces in a very natural way an element of temporal coherence to the stochastic variability. Further temporal and spatial coherence is inherent to the scheme, in that it is explicitly designed to operate with non-local inputs, as we discuss shortly. The extent of the non-locality is likely to be important for the upscale impact of the stochastic fluctuations (e.g. Buizza *et al.*, 1999). A source of noise that was entirely independent for each model grid point and time step may be largely washed out through numerical diffusion, however physical the noise source might be. The experiments described here will establish the impact of coherency that arises from intrinsic, physical correlation scales of deep convection.

At each time step clouds that have been present for time  $T_L$  are removed, and new clouds are initiated. The KF plume model is used to compute vertical profiles of convective tendencies for each cloud and these are summed over all the clouds to feed back to the model dynamics. If the size of the grid box is large enough then it will contain a representative sample of the full spectrum of clouds, and the tendencies will tend to those from a deterministic scheme; in this case then the grid-box state will provide a good approximation to the large-scale environmental state and can be used directly in order to compute  $\langle M \rangle$ .

More generally, time and space averaging across multiple grid boxes is necessary in order to obtain a large-scale state suitable for use in the computation of the closure. By definition, the cloud-base mass flux to be computed as the closure of any mass-flux parametrization is a function

of the large-scale forcing (Plant, 2010). Conventionally, the local, instantaneous grid-box state is used to approximate the large-scale environment. However, the grid-box state is subject to fluctuations as traditional deterministic parametrizations often produce on-off behaviour and strong time step-to-time step variability (Willett and Milton, 2006; Stiller, 2009). In order to remove these fluctuations, and so obtain a large-scale environmental state from which  $\langle M \rangle$  can properly be calculated, the grid-scale atmospheric state should be averaged in space and in time, over neighbouring grid points and recent time values. This averaging must be over a sufficient number of points that the resulting  $\langle M \rangle$  can indeed be identified with the ensemble-mean total mass flux for the large-scale environment, but not over so many points that a significant fraction of them are not representative of the large-scale environment represented by the grid point at which the convection is being calculated (it should be emphasized that the averaging is not intended to transmit information about the environment at distant grid boxes to the grid box in question; rather to use distant grid boxes to provide more information about the environment at the grid box in question). In other words, the necessary averaging should not obscure genuine variations in the large-scale forcing. It is not at all obvious that both conditions can be satisfied simultaneously to produce a suitable slowly varying  $\langle M \rangle$ —a point to be tested explicitly here.

For stochastic parametrizations such as PC, in which fluctuations are predicted and controlled, then the importance of the distinction between the grid-box state and the large-scale state is readily apparent. However, we stress that the distinction is potentially an important one for the representation of any parametrized process which does not have a clear scale separation between the intrinsic scales of the process and the grid scale. This point has actually been recognized for some time (e.g., Lander and Hoskins, 1997; Kuo *et al.*, 1997, p. 477) but practitioners have so far shied away from the natural consequence that aspects of parametrization should be non-local.

In the PC scheme, the basis for the closure is the removal of CAPE, following KF and several other parametrizations (e.g. Zhang and McFarlane, 1995; Bechtold *et al.*, 2008). Specifically,  $\langle M \rangle$  is defined as the total mass flux required to remove 90% of CAPE through the action of convection within a closure time  $T_c$ . An appropriate value for  $T_c$  is discussed in section 2.4.

### 2.3. Averaging scales

Studies by Ricciardulli and Sardeshmukh (2002) and Smith *et al.* (2005) suggest that the spatial correlation length of tropical convection on a 3-hourly time-scale is of the order of 120 km (we interpret the term ‘correlation length’ here to mean lengths over which variations in the large-scale environment are not significant). The number varies somewhat over different regions (and is generally slightly higher over the oceans than over land). These studies suggest that variations of the large-scale environment for convection are rather modest on scales of around 100 km, and so we might consider this to be a suitable upper limit for spatial averaging (in each direction) of the input to a closure calculation, in order to ensure that variations of the large-scale environment within the averaging area do not adversely affect the calculation. Another study which lends support to this proposal is that of Moron *et al.* (2007), who found that

the correlation scale for tropical rain amounts on wet days, on daily time-scales, is never more than about 100 km.

On the other hand, the spatial averaging must also be sufficient to smooth out local fluctuations that we would not wish to consider as part of the large-scale environment. The CRM study by Shutts and Palmer (2007) found that coarse-graining at a scale of 120 km or less was required in order to obtain the full range of convective behaviour, in an idealized experiment relevant to the Tropics. Domain sizes of a similar order of magnitude have been successfully used in many CRM experiments (e.g. Robe and Emanuel, 1996; Shutts and Gray, 1999; Cohen and Craig, 2006; Davies, 2008; Davoudi *et al.*, 2010), suggesting that it should indeed be possible to obtain sufficient statistical averaging on a scale of around 100 km.

The studies of Ricciardulli and Sardeshmukh (2002) and Holloway and Neelin (2010) estimate typical durations of ‘wet events’ and autocorrelation time-scales for tropical precipitation to be of the order of a few hours. Following similar reasoning as for the spatial averaging, these correlation times provide a suitable upper limit for the temporal averaging that might reasonably be used for the input to the closure calculations of a parametrization. Variations of the large-scale environment should be rather modest on scales of less than a few hours, but one would not wish to take an average over longer time-scales on which the diurnal variation of land surface temperature (for example) would become a significant aspect of the large-scale environmental forcing for convection.

Subject to the above upper limits on averaging scales, a major purpose of this paper is to determine practical lower limits for averaging scales that are required in order to obtain an accurate estimate of  $\langle M \rangle$  in the CAPE closure calculations, as judged by the ability of the PC scheme to yield the correct theoretical equilibrium PDF for  $M$  (i.e. that which is self-consistent with its design principles). The set-up used for doing this is described in the next subsection.

### 2.4. Radiative–convective equilibrium set-up

The set-up used to investigate the statistics of parametrized convection is an idealized configuration of the UK Met Office Unified Model (Davies *et al.*, 2005, MetUM), running at version 6.1. The boundary layer and large-scale cloud parametrizations are used with the standard settings of the MetUM, as described in Lock *et al.* (2000) and Wilson and Ballard (1999), respectively.

We use the term radiative–convective equilibrium in its generic sense, as being the outcome from integrating a model of convection for a long period with a time-invariant forcing being imposed. By forcing we refer to any process that would act to destabilize the atmosphere in the absence of convective activity. The forcing imposed is extremely simple here, a fixed tropospheric cooling rate being applied as follows:

$$\left. \frac{\partial T}{\partial t} \right|_{\text{forced}} = \begin{cases} -\dot{T}_0 & p > 2p_0 \\ \dot{T}_0(p_0 - p)/p_0 & 2p_0 > p > p_0 \\ 0 & p_0 > p, \end{cases} \quad (8)$$

where  $p_0 = 200$  hPa and  $\dot{T}_0$  is a constant defining the strength of the forcing. The domain is a homogeneous sea surface with a constant sea surface temperature of 300 K. The

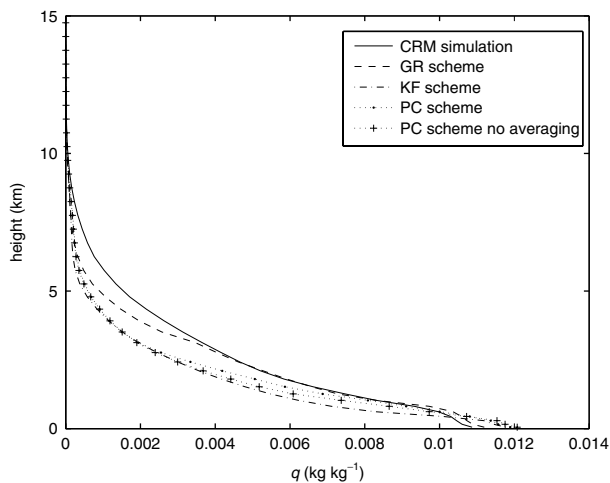


**Figure 1.** Mean vertical profiles of water vapour  $q$  in radiative-convective equilibrium experiments with 8 K per day imposed cooling. Results are shown for a cloud-resolving model study (CRM, solid line) and for MetUM experiments using the Gregory–Rowntree scheme (GR, dashed line), the Kain–Fritsch scheme (KF, dash-dotted line) and the Plant–Craig scheme (PC, dotted lines). Results from the PC scheme are shown for standard averaging (dotted line with points) and for no averaging (dotted line with pluses).

Coriolis parameter is set to zero. There is no wind profile imposed in the simulations, and so all winds that occur are induced by the convection.

The domain is three-dimensional and of size 512 km in each horizontal direction. Bicyclic boundary conditions are applied. The default choices for the grid length and the cooling rate are 32 km and  $\dot{T}_0 = 8$  K per day, respectively, although other choices, namely 16 and 51.2 km for the grid length, and 10 and 12 K per day for the cooling rate, are also explored. The model has 49 levels in the vertical. The initial conditions were a horizontally homogeneous atmosphere at rest, with vertical profiles of temperature and moisture being taken from the equilibrium state of an equivalent CRM experiment by Cohen and Craig (2006), which is forced in the same way and has a tropospheric cooling rate of  $\dot{T}_0 = 8$  K per day. The CRM profile is plotted in Figures 1 and 2. Since the initial conditions were from a state of RCE, albeit from a different model, the MetUM was able to reach its own RCE state rather quickly, and all MetUM simulations had reliably reached equilibrium after five days. The simulations were each run for 25 days.

It is somewhat unusual, but by no means unprecedented, to perform idealized RCE experiments at resolutions which require convection to be parametrized. Given that almost all convective parametrizations are based on quasi-equilibrium thinking (Emanuel, 2000), it is perhaps surprising that such tests are not a standard part of parametrization development, and given that the tests are far from trivial we echo the remarks of Held *et al.* (2007) that further studies with such configurations would be beneficial. In the present context, we assert that a convective parametrization must behave in accordance with its own design principles in an RCE configuration, or else it is scarcely likely to behave adequately in more complex situations. Alongside runs with the PC scheme, we have also performed comparison experiments with the KF scheme, and with the standard convection scheme of the MetUM, as described in Martin *et al.* (2006) and based on the scheme of Gregory and Rowntree (1990, hereinafter GR). Previous studies using a convection

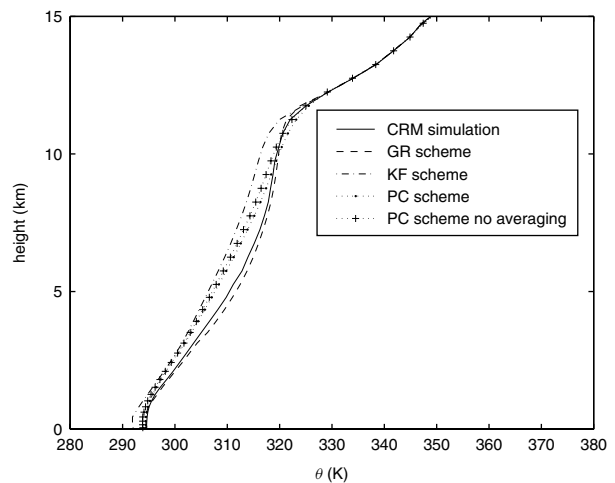


**Figure 2.** As Figure 1 but showing mean vertical profiles of potential temperature  $\theta$ .

parametrization in a similar RCE set-up have focused on the organized structures that are established in large domains with interactive radiation (e.g. Held *et al.*, 2007; Held and Zhao, 2008). The study of Larson and Hartmann (2003) also employed interactive radiation, and demonstrated that the KF parametrization is capable of producing a realistic large-scale mean state in such experiments, at least in terms of its response to changes in sea surface temperature.

As discussed by Held *et al.* (2007), RCE experiments with parametrized convection can exhibit ‘grid-point storms’ if an instability is not removed by the convection scheme, but is instead manifest as intense localized precipitation produced by the large-scale cloud parametrization. Preliminary experiments with our set-up showed that the simplest way to eliminate such storms was to choose a sufficiently short CAPE closure time-scale  $T_c$ . However, it was also found that with too short a  $T_c$  the convection scheme responds too strongly and ‘overcompensates’, leading to oscillations in the rainfall, even if averaged over the whole domain. The simulations to be presented here use a constant  $T_c = 75$  min, except for the case with a 51.2 km grid length, where a value of 120 min is used. These values are compatible with the range of values found in the convective parametrization literature. Moreover, a systematic reduction in the closure time scale with reducing grid length has been found to be beneficial for the partitioning between convective and large-scale processes in the ECMWF model (Bechtold *et al.*, 2008)—a point that seems likely to be related to the systematic increases in the vertical velocities of explicitly resolved motions at reduced grid lengths (e.g. Paulius and Garner, 2006).

The numerical experiments will determine whether the PC scheme can reproduce the theoretically expected PDF of total mass flux  $M$  (Eq. (2)) under large-scale forcing conditions for which the theory holds. The idealized set-up used here provides just such conditions, the fixed cooling ensuring that once the system has reached equilibrium the total mass flux  $\langle M \rangle$  required to balance the forcing is constant. Under these conditions, the upper limit on an acceptable averaging area is removed since at all times the entire domain is representative of the same large-scale environment. This allows us to determine the lower limits for temporal and spatial averaging of the input to the closure calculations that are required in order to obtain a sufficiently

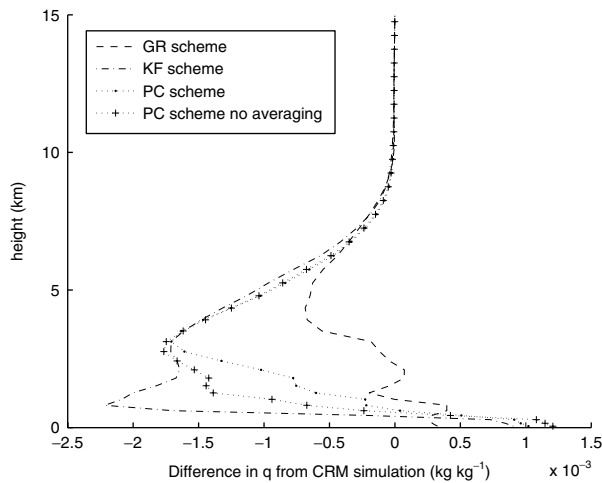


**Figure 3.** Vertical profiles of the difference between water vapour  $q$  from MetUM experiments with parametrized convection scheme and from a corresponding CRM experiment. Results are shown using the Gregory–Rowntree scheme (GR, dashed line), the Kain–Fritsch scheme (KF, dash-dotted line) and the Plant–Craig scheme (PC, dotted line). Results from the PC scheme are shown for standard averaging (dotted line with points) and for no averaging (dotted line with pluses).

accurate representation of the large-scale environment at each grid box and time step, so that  $\langle M \rangle$  as computed by the closure is sufficiently steady to allow the PC scheme to reproduce Eq. (2). As an additional test on the theory, and its implementation in the PC scheme, we will also investigate whether the PDF of mass flux per cloud (Eq. (1)), can be reproduced. Although this PDF is imposed by the PC scheme at the LCL, that is not the case at other heights.

### 3. Results for equilibrium state

#### 3.1. Mean profiles

Before considering the mass-flux fluctuations produced by the stochastic parametrization scheme, we first test its ability to produce appropriate mean profiles. For the idealized RCE configuration studied here, a suitable comparison is provided by the results from the corresponding CRM experiment by Cohen and Craig (2006). Vertical profiles of water vapour  $q$  and potential temperature  $\theta$  are shown in Figures 1 and 2, respectively, for the CRM study and for the three convection schemes used in the current MetUM experiments. The profiles have been averaged over the full model domain in each case, and also daily over the last 20 days of the simulations. The time variations amongst domain-mean profiles were found to be modest, and certainly no larger than the variation amongst the results for different convection schemes. The averaging strategy for the input to the closure calculations of the PC scheme that has been used here is the ‘standard averaging’, to be fully specified in section 3.3. Also shown are the results from an experiment with the PC scheme and grid-scale input only, i.e. with no space or time averaging of the input.

Also shown, in Figures 3 and 4, are the differences between the various profiles produced by the MetUM experiments with parametrized convection and the corresponding CRM profiles. The magnitudes of these differences are similar to those found in corresponding single-column model (SCM) experiments with the MetUM (Plant and Craig, 2008).

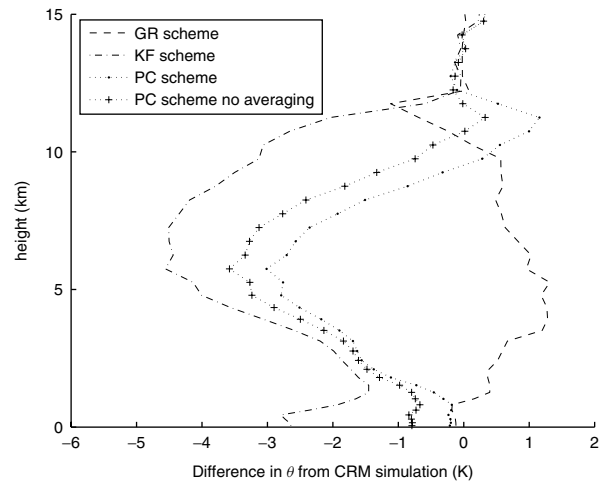


**Figure 4.** As Figure 3 but showing vertical profiles of the differences in potential temperature  $\theta$ .

In the current three-dimensional experiments the lower atmosphere is drier than that of the CRM, whereas it was moister in the earlier SCM experiments. The difference is likely to be due to the different treatments of surface fluxes. In the current experiments the surface fluxes are computed from bulk aerodynamic formulae and so are dependent on the near-surface wind speeds that develop in the simulations. The relative dryness suggests that such wind speeds tend to be somewhat weaker than in the CRM. By contrast, the surface fluxes in the comparison SCM were simply taken to be proportional to the moisture difference across the surface layer, with a fixed, predefined constant of proportionality (Plant and Craig, 2008).

The GR scheme yields ‘better’ profiles than the KF scheme (i.e. closer to the CRM results). The profiles from the PC scheme are intermediate between those of the GR and KF schemes, although it is closer to the KF result. This is scarcely a surprise given that it is based on the same plume model and so is essentially a spectral and stochastic generalization of the KF scheme. Averaging the input to the closure calculations of the PC scheme has little effect on the mean state produced, with a small improvement over the experiment with no averaging.

#### 3.2. Vertical profile of mean mass flux per cloud

The vertical profile of mean mass flux per cloud is plotted in Figure 5 in order to establish the context for the following results. The profile is plotted with different averaging strategies having been applied to the input of the closure calculations of the PC scheme. The strategies will be fully described in the following subsection. For the present purposes, it is sufficient to note simply that the averaging strategy chosen has little effect on this profile.

The profile can be compared with that of the PC scheme in the SCM (Plant and Craig, 2008, their figure 8). The behaviour is broadly similar, although the current experiments have a lower LCL (recall that  $\langle m \rangle = 2 \times 10^7 \text{ kg s}^{-1}$  is imposed at the LCL) than in the SCM, and show a smoother increase with height of the mean mass flux per cloud. The peak value of  $\langle m \rangle(z)$  is similar but occurs at just over 8 km in these three-dimensional experiments rather than at just below 10 km in the SCM.



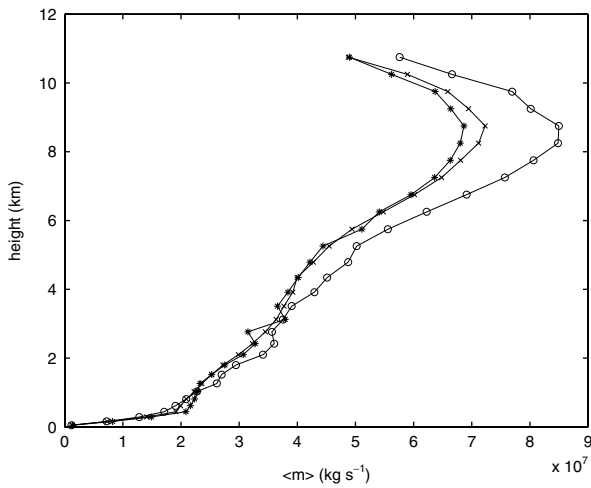


**Figure 5.** Vertical profile of the mean mass flux per cloud for three different averaging strategies applied to the input of the PC scheme. The strategies are described as no-averaging (open circles), standard-averaging and maximal-averaging (stars) and are detailed in section 3.3. The values were obtained by averaging the mass flux of every convective plume present at each model level, starting from five days into the simulation and continuing until data for 1300 clouds had been recorded.

### 3.3. Development of averaging strategy

We consider first an experiment with a grid length of 32 km and a forcing  $\dot{T}_0 = 8$  K per day, along with a ‘maximal’ averaging strategy for the input to the PC scheme. Specifically, the closure calculations of the scheme were performed on profiles averaged temporally over 63 min, and averaged spatially over the grid box in question and its neighbours up to seven grid boxes away. Thus the averaging area was a square of side 480 km, encompassing almost the entire model domain. All grid boxes within the averaging area and all time steps within the averaging period were treated equally, i.e. no weighting functions were applied in constructing the averages.

Figure 6(a) shows a PDF obtained at 1.52 km for the mass flux per cloud,  $m$ . This height was chosen as it is above the LCL but low enough such that almost all plumes launched by the PC scheme are still buoyant and so will contribute to the PDF. The PDF was constructed from values for the mass flux of each cloud present in the domain recorded at 6-hourly intervals for a period of 20 days. The PDF agrees well with the theoretical prediction from Eq. (1), as do the results obtained for other heights (not shown).

A PDF for  $M$ , the total convective mass flux, is shown in Figure 6(b). The totals are for areas of 64 km<sup>2</sup> and were computed by partitioning the domain into  $8 \times 8$  sub-domains (each containing  $2 \times 2$  grid boxes) and summing over plumes within each sub-domain. The same time sampling was used as above, giving a total of 5184 values of  $M$  for use in constructing the plot shown. Again, the numerical results agree well with the theory, and agreement also holds good for other heights and over other sizes of the horizontal area.

The agreement with theory for the maximal-averaging strategy is a valuable result, which demonstrates that the PC scheme is providing a correct implementation of its underpinning theory when embedded within a full three-dimensional atmospheric model. We now examine whether this remains the case when the degree of averaging is reduced, thereby testing whether the scheme will be capable

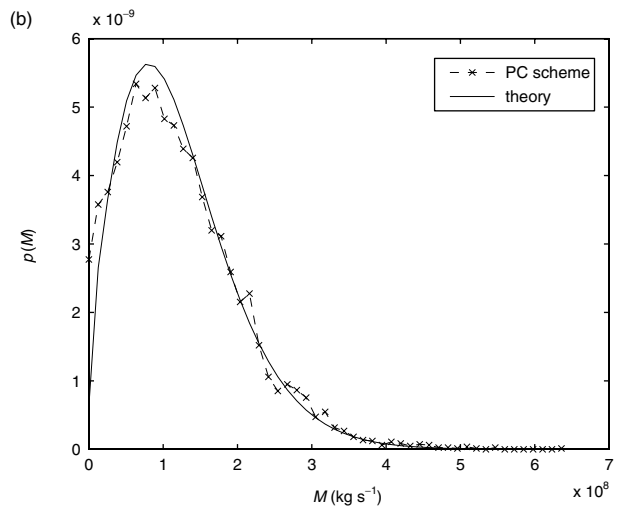
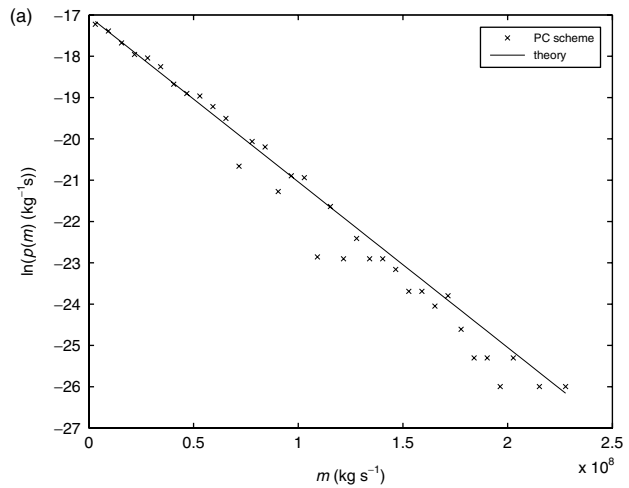


**Figure 6.** PDFs at a height of 1.52 km (a) for the mass flux per cloud,  $m$ , and (b) for the total mass flux  $M$  over the horizontal area 64 km<sup>2</sup>. The crosses show results from a simulation with the PC scheme for a grid length of 32 km, an imposed cooling of  $\dot{T}_0 = 8$  K per day and the maximal-averaging strategy described in the main text. Also shown are the theoretical predictions (solid lines) given by Eqs (1) and (2), evaluated using values for  $\langle m \rangle$  and  $\langle M \rangle$  computed directly from the model data. The bin width for  $m$ , and all similar plots in this paper, is  $\langle m \rangle / 4$  (i.e. dependent on the average value for that particular plot), and the bin width for  $M$ , and all similar plots in this paper, is such that there are 51 equally spaced bins from the minimum to the maximum value of  $M$  inclusive.

of accommodating variations in the large-scale forcing. Experiments have been performed for various combinations of temporal and spatial averaging. In each case the temporal averaging combines the current state of the atmosphere with its state at previous time steps, while the spatial-averaging domain is composed of a square with the grid point of interest in the centre and a whole number of grid boxes along each side.

A summary of the experiments performed is shown in Table I, alongside two measures of the fit to theory obtained for the PDF of  $M$  at 1.52 km. The third column of the table lists the correlation coefficient between the model data for each bin and the theoretical value obtained from Eq. (2). The fourth column shows the normalized variance of  $M$ , which should be equal to 2 according to Eq. (3), when the PC scheme works correctly according to its underlying theory. It is clear from both the measures in the table that increased spatial averaging improves the agreement with theory. The

Table I. List of experiments performed in order to test averaging strategies for the input to the closure calculations of the PC scheme. In each case the model grid length was 32 km and the cooling rate was  $\dot{T}_0 = 8$  K per day.

Space avg. (km)	Time avg. (min)	Correlation coefficient	Normalized variance
32	1	0.866	2.58
96	50	0.895	2.18
160	1	0.942	2.05
160	20	0.927	2.07
160	50	0.940	2.02
160	120	0.948	2.09
160	200	0.931	2.04
480	63	0.982	2.08

The first two columns show the length of the side of the averaging square, and the averaging time period respectively. The third column gives the correlation coefficient between the experimental PDF of  $M$  over an area of  $64 \text{ km}^2$  at  $1.52 \text{ km}$  and the theoretically expected PDF. The fourth column gives the normalized variance of total mass flux,  $\langle (M - \langle M \rangle)^2 \rangle / (\langle M \rangle \langle m \rangle)$ , calculated from the simulation results at the same height.

time averaging is less important, and does not produce clear systematic differences in the two measures.

Note that the last line of Table I corresponds to the maximal averaging strategy discussed earlier, while the first line corresponds to a case of no averaging, with the parametrization relying only on local, instantaneous input as in a traditional approach. As shown explicitly in Figure 7, there are clear departures from theory if no averaging is performed. This arises because (by design for a stochastic scheme, but also in practice for a deterministic mass flux scheme) there are local fluctuations in the profiles. If local profiles are used as a basis for closure calculations then those calculations will be distorted by the fluctuations, thereby introducing an artificial source of variance. We reiterate that the theoretical basis of a quasi-equilibrium closure requires that the closure depends on the large-scale environment for which the grid-scale state is not necessarily a good approximation.

Based on these results, an averaging domain of side 160 km and an averaging time of 50 min were chosen to define the ‘standard’ averaging strategy for use in the remainder of this paper. Figure 8 shows the agreement with theory for this standard averaging, which is clearly improved over the case of no averaging (Figure 7), and not too much worse than that for maximal averaging (Figure 6). Thus the standard averaging is judged to be sufficient to obtain good agreement with the theory, but it nonetheless would allow for variations in the large-scale forcing to be captured, respecting the arguments based on observed correlation scales in section 2.3.

### 3.4. Implementation of averaging strategy for other test cases

The standard-averaging strategy developed in the previous subsection was also adapted for use in experiments with different strengths of forcing and with different grid lengths. Specifically, experiments have been performed using  $\dot{T}_0 = 10$  and  $\dot{T}_0 = 12$  K per day, as well as with the original amplitude of cooling but with grid lengths of 16 and 51.2 km.

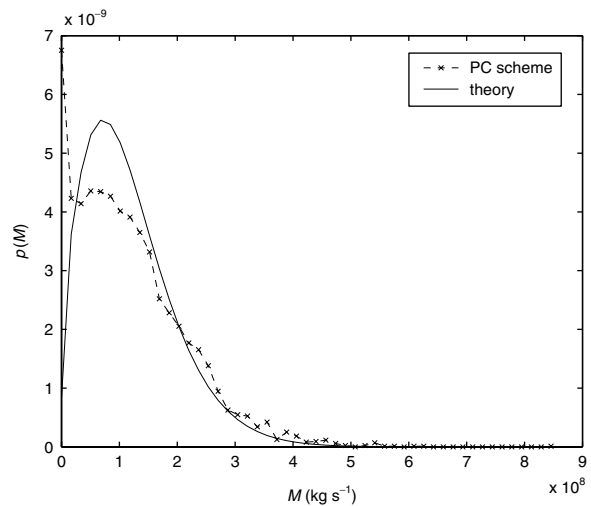


Figure 7. PDF at a height of 1.52 km for the total mass flux  $M$  over the horizontal area  $64 \text{ km}^2$ . The crosses show results from a simulation with the PC scheme for a grid length of 32 km, a cooling of  $\dot{T}_0 = 8$  K per day and no averaging in the input to the scheme. Also shown is the theoretical prediction (solid line) given by Eq. (2), evaluated using values for  $\langle m \rangle$  and  $\langle M \rangle$  computed directly from the model data.

Table II. Averaging strategies used for the experiments described in section 3.4.

Experiment	Space average (km)	Time average (min)
$\dot{T}_0 = 10$ K per day	160	40
$\dot{T}_0 = 12$ K per day	160	33
Grid spacing 16 km	144	67
Grid spacing 51.2 km	153.6	51

The second column shows the length of the side of the averaging square, and the third column shows the averaging time period.

The adaptations of the averaging strategy for these experiments are detailed in Table II. The adaptations for different grid spacings (bottom two rows) are entirely for technical reasons, since the spatial averaging is performed over a square with a whole number of grid boxes on each side. The time averages for different grid spacings vary somewhat because different time steps were used for different grid spacings. The adaptations for different forcings (top two rows), on the other hand, arise because, for stronger forcing, the number of clouds produced increases proportionally (given that the mass flux per cloud  $\langle m \rangle$  remains constant). It is therefore possible to reduce the averaging area and/or period, and still average over an equivalent number of clouds. In practice, the temporal averaging was reduced proportionally to account for this point, the decision being dictated by the fact that the averaging square could only be reduced in size by rather large discrete steps.

The resulting PDFs from the experiment with a cooling rate of  $\dot{T}_0 = 12$  K per day are shown in Figure 9. There is good agreement with the theoretical curves, as was also found in the experiment with a cooling rate of  $\dot{T}_0 = 10$  K per day (results not shown). Thus the PC scheme is able to reproduce the correct mass-flux variability for different forcing conditions.

Results with grid lengths of 16 and 51.2 km are shown in Figures 10 and 11, respectively. The PDFs for  $M$  in

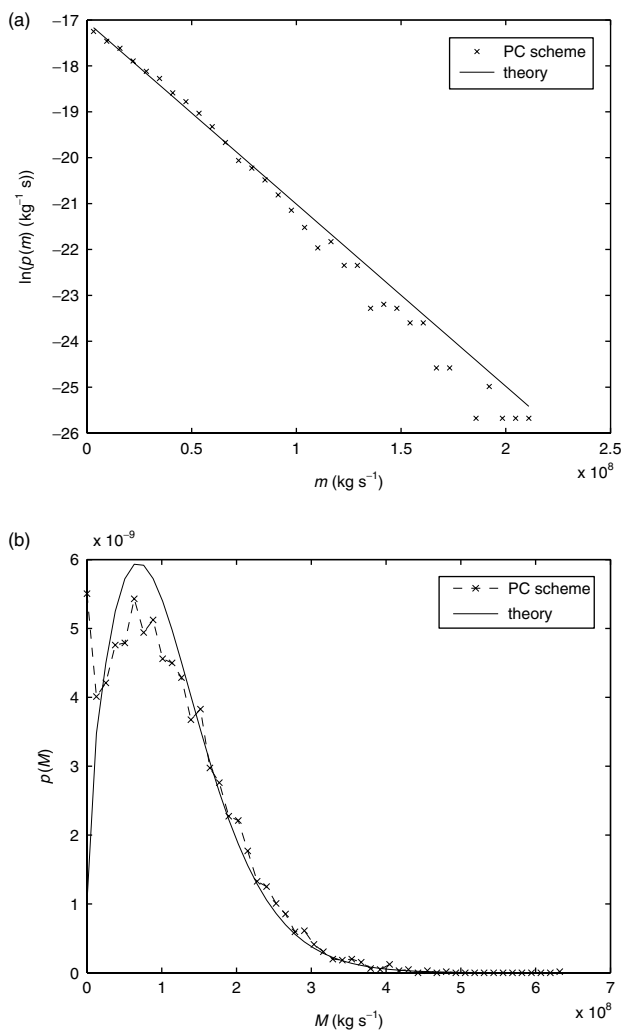


**Figure 8.** As Figure 6, but for the standard-averaging strategy described in the main text.

these figures are for areas of  $64 \text{ km}^2$  (a partition into  $8 \times 8$  sub-domains containing  $4 \times 4$  grid boxes) and  $102.4 \text{ km}^2$  (a partition into  $5 \times 5$  sub-domains containing  $2 \times 2$  grid boxes), respectively. The agreement with theory is again good, demonstrating that the PC scheme adapts correctly to different resolutions.

### 3.5. Results at other heights

Mass-flux statistics from the PC scheme have so far been presented for a height of 1.52 km. The underpinning theory is not dependent on the height in question, so it is important to investigate whether the scheme is providing a correct implementation of the theory for other heights. In this subsection we investigate whether or not  $m$  follows an exponential distribution at higher levels and how well Eqs (2) and (3) describe the distribution of  $M$ . Results are shown for the experiment with 32 km grid length,  $\dot{T}_0 = 8 \text{ K}$  per day cooling rate and the standard-averaging strategy of section 3.3.

Figure 12 shows PDFs of  $m$  at 3.51 and 8.75 km. In both cases these agree with the exponential shape predicted by theory. A more detailed assessment of this agreement is found in Figure 13. This shows the correlation coefficient between the probabilities taken from the model data and the probabilities taken from Eq. (1) for the same mean mass

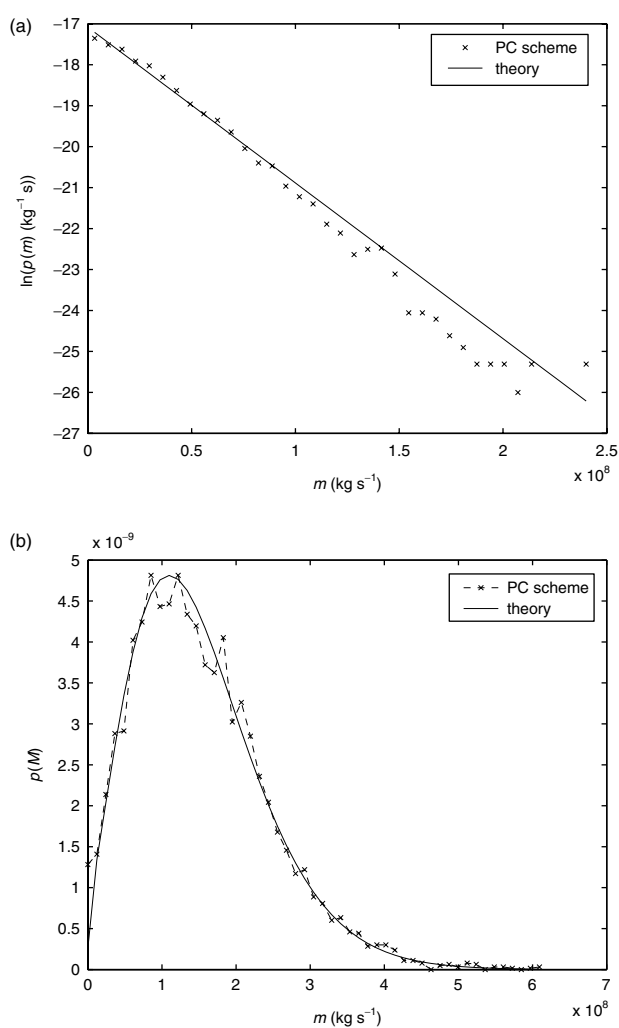


**Figure 9.** As Figure 6, but for a cooling rate of  $\dot{T}_0 = 12 \text{ K}$  per day, and using the averaging strategy as specified in Table II.

flux,  $\langle m \rangle$ . The agreement is slightly worse at the highest levels: this is likely to be due to the fact that there are fewer surviving clouds contributing to the experimental statistics, and that clouds with different strengths have different likelihoods of surviving to the top of the troposphere. It is also slightly worse at around 7 km, where there are anomalously very slightly fewer strong clouds than in the corresponding exponential distribution. However, the correlation coefficient nonetheless remains above 0.9 at all heights.

The ability of the underlying theory to describe the distribution of  $M$  at different heights is shown in Figure 14. This displays the correlation coefficient between probabilities predicted by Eq. (2) and normalized number frequencies taken from the data: the coefficients are computed in the same way as those discussed in section 3.3. Results were obtained using four different-sized groups of grid boxes: for example, the results for an area of  $128 \text{ km}^2$  were obtained by dividing the domain into  $4 \times 4$  groups, each of  $4 \times 4$  grid boxes.

The graph in Figure 14 displays some interesting nonlinearities in the coefficient with both height and averaging area. On inspection of individual PDF comparisons (not shown), it is apparent that, away from the LCL, the Cohen–Craig theory is less well adhered to when there is an intermediate number of areas with zero mass flux—in this case instances

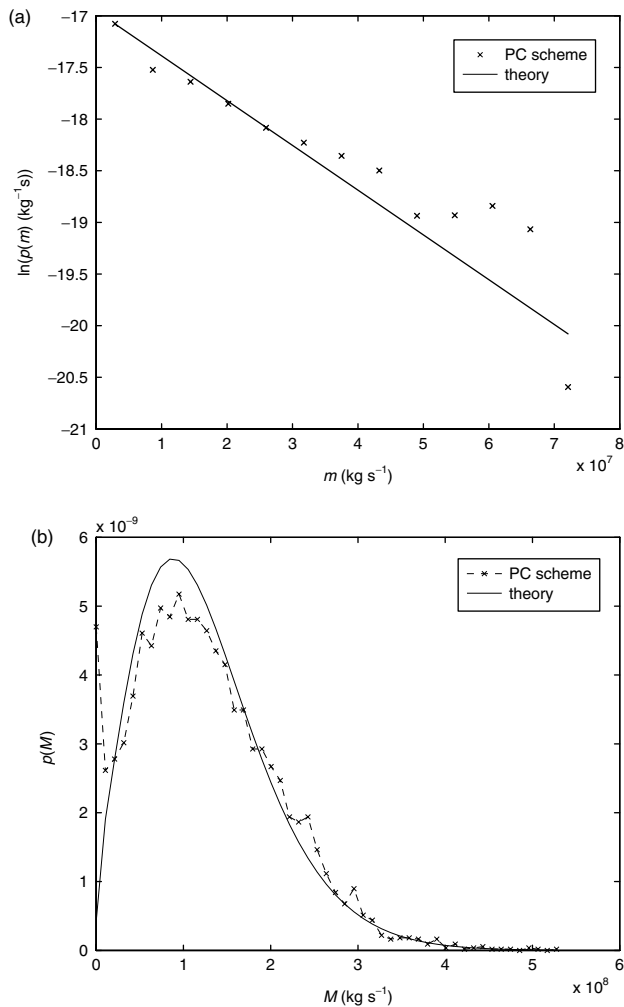


Figure 10. As Figure 6, but for a model grid length of 16 km, and using the averaging strategy as specified in Table II.

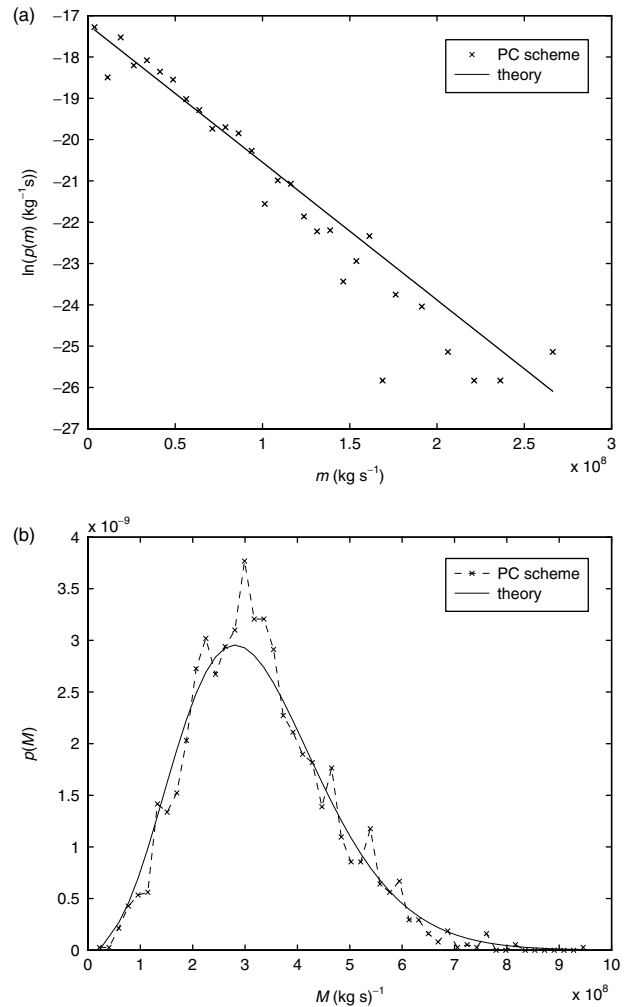


Figure 11. As Figure 6, but for a model grid length of 51.2 km, and using the averaging strategy as specified in Table II. The PDF of  $M$  in (b) is over a horizontal area of  $102.4 \text{ km}^2$ .

of zero  $M$  are overestimated and instances of low  $M$  are underestimated. For the smallest area size, 32 km, the PDF is dominated by instances of zero  $M$  at cloud base, and this does not change higher up as clouds disappear. However, looking at the 64 km areas, the theory is well adhered to near to cloud base, but the clouds seem to disappear in ‘clusters’, so that there are too many instances where all the clouds in an area have disappeared (and too many where no clouds have disappeared) relative to what would be expected if they were to disappear uniformly. Higher up still, the uniformity is restored, and the PDF is now dominated by instances of zero  $M$ , similar to with the 32 km area at all heights. For the 128 km area, a similar phenomenon occurs: lower down, there are no instances at all of zero  $M$  (as the area is sufficiently large always to capture at least one cloud), but as the clouds disappear with height the distribution crosses into the intermediate range, which is less well captured by the theory. Finally, the relatively low values when dividing the domain into four  $256 \text{ km}^2$  areas are at least partly attributable to the fact that the quantity of experimental data is relatively low.

The normalized variance,  $\langle (M - \langle M \rangle)^2 \rangle / (\langle M \rangle \langle m \rangle)$ , is plotted as a function of height in Figure 15, for values of  $M$  determined at the level of the individual grid box. This further demonstrates the agreement with the underlying theory, to a similar extent as the agreement obtained from CRM data (Cohen and Craig, 2006). Thus, although the

PC scheme imposes the theoretical distribution at the LCL, the underlying theory remains appropriate to describe the distributions that are produced at all heights.

#### 4. Rainfall statistics

Bulk mass flux schemes such as Gregory and Rowntree (1990) and Kain (2004) consider a single, effective cloud rather than a spectrum of clouds carrying different mass fluxes (Plant, 2010). Such schemes therefore do not yield explicit results for  $m$ . In order to compare the convective fluctuations produced by different convection schemes, it is therefore more convenient to consider fluctuations in rainfall rather than mass flux. Following Shutts and Palmer (2007), the Craig and Cohen (2006) theory can be generalized for convective rainfall, since the same important equilibrium constraints apply to this variable as to the mass flux. Specifically, in the absence of any large-scale contribution to the rainfall, at equilibrium the ensemble-mean total convective rainfall must balance the (evaporative) moisture source. Moreover, the total rainfall is comprised of contributions from a variable but finite number of approximately independent rain sources. Thus a similar distribution to Eq. (2) is expected to describe the statistics

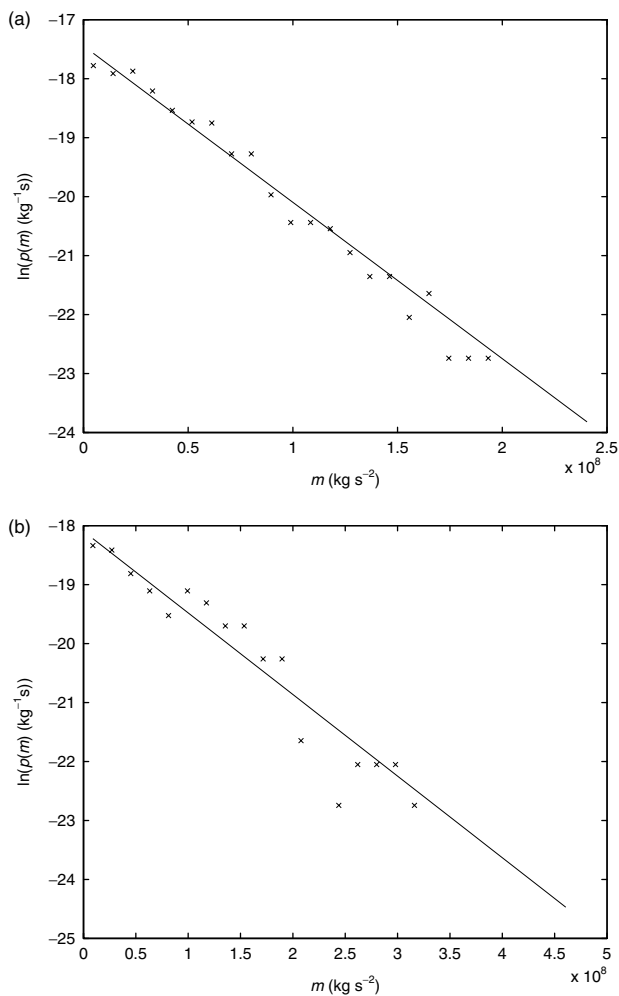


Figure 12. PDFs of  $m$  at heights of 3.51 km (a) and 8.75 km (b). Clouds that were produced by the parametrization, but which did not reach the height in question, are not included.

of the convective rainfall:

$$p(C) = \delta(C) e^{-\frac{C}{\langle C \rangle}} + \frac{1}{\langle C \rangle} \sqrt{\frac{\langle C \rangle}{C}} e^{-\frac{C+\langle C \rangle}{\langle C \rangle}} I_1 \left( \frac{2}{\langle C \rangle} \sqrt{C \langle C \rangle} \right), \quad (9)$$

where  $C$  is the total rainfall within a given area, and  $c$  is the rainfall produced from each contributing source.

Rainfall data produced by each of the Plant–Craig (PC), Kain–Fritsch (KF) and Gregory–Rowntree (GR) schemes were used to construct frequency distributions for the total rainfall over various horizontal areas. Rainfall values were recorded every 8 hours for a total of 20 days, for each scheme. Results from the PC scheme are presented in Figure 16, in which they are also compared with Eq. (9). The focus here is on the scaling of the distribution with area. Thus a suitable value to choose for  $\langle c \rangle$  in plotting the theoretical curves is that obtained by fitting the experimental data obtained at 256 km<sup>2</sup> to Eq. (9) (separately for each scheme, with  $\langle C \rangle$  being prescribed simply from the mean of the experimental data). The resulting value for  $\langle c \rangle$  was then used to produce the theoretical curves for the other three areas.

The agreement with theory for the PC scheme is generally good, a highly non-trivial result for this change of fluctuating variable. The exception is at the grid scale itself, where there are too many instances of light rain. Given that the

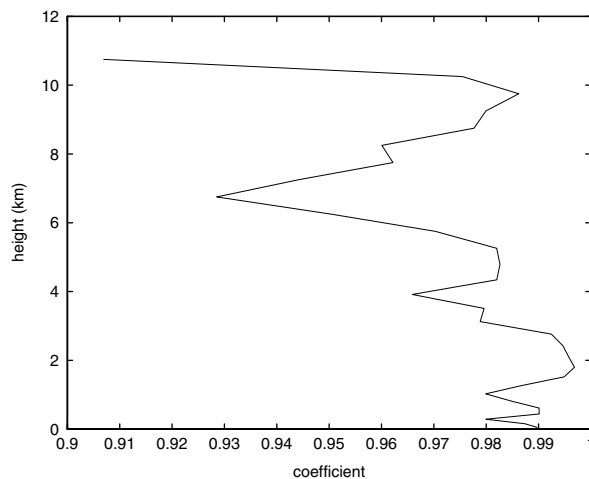


Figure 13. Correlation coefficient between theoretical and experimental PDFs of  $m$ , as a function of height.

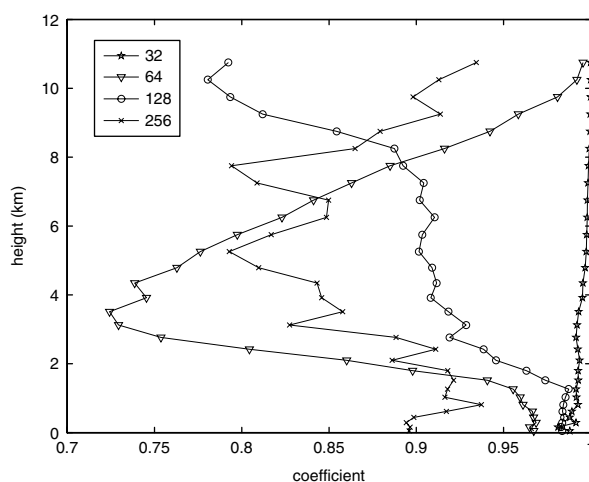


Figure 14. Correlation coefficients between theoretical and experimental PDFs of  $M$ , as a function of height. The PDFs were constructed for horizontal areas of 32 km<sup>2</sup> (stars), 64 km<sup>2</sup> (triangles), 128 km<sup>2</sup> (circles) and 256 km<sup>2</sup> (crosses).

scheme imposes the theoretical distribution of cloud-base mass flux at the grid scale and, given that the rainfall scales appropriately with area over larger areas, it becomes tempting to hypothesize that this may point to a problem with the implicit mass-flux–rainfall relationship that is produced by the plume model being used. However, any modifications to the plume model which might improve the situation are beyond the scope of the present study.

Table III compares the results from the PC scheme with those of the KF and GR schemes. The correlation coefficient, used in previous sections, was found not to discriminate sufficiently the level of agreement between Eq. (9) and the experimental data, particularly with the smaller areas, over which instances of zero rainfall are an important aspect of the PDF. Therefore, another measure has been adopted for assessing the agreement between theory and experiment. It is obtained simply by calculating the total area between the two PDFs:

$$A = \sum_i |p(C_i) dC - v_i / N_{\text{data}}|, \quad (10)$$

where  $i$  labels the bin,  $v_i$  is the number of data points in bin  $i$  and  $N_{\text{data}}$  is the total number of data points. This measure

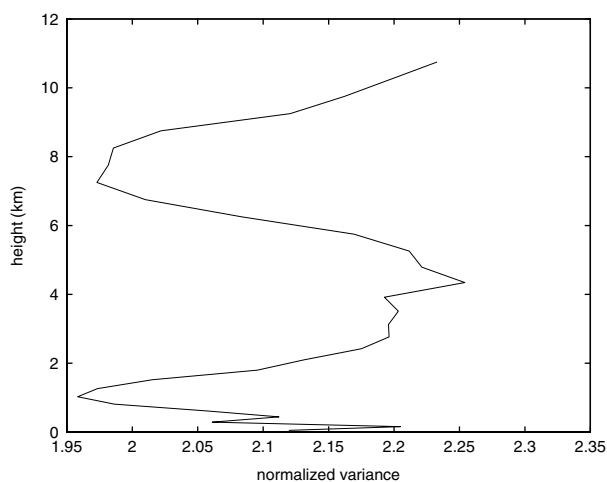


Figure 15. Variation of normalized variance  $\langle (M - \langle M \rangle)^2 \rangle / (\langle M \rangle \langle m \rangle)$  with height, for  $M$  determined from individual grid-box values.

should not, in principle, require any normalization because the total area under the PDFs is always unity. However, care must be taken that the sampling of the data (in particular the number of bins and the upper and lower limits) is done in the same way for each scheme for a fair comparison to be made. Here, the number of bins was set to be equal to the number of data points divided by 10, subject to a minimum of 100 and a maximum of 500. The lower limit was always set at zero and the upper limit such that 99.5% of the area under the theoretical PDF was included within the limits.

The PC scheme does the best job of rescaling the theoretical rainfall distribution across the different areas (a lower value of  $A$  denotes a better agreement between theory and experiment). Perhaps unsurprisingly, all three schemes perform well at the largest scale, at which  $\langle c \rangle$  has been fit and for which a deterministic, 'single effective cloud' method should be appropriate. At the grid scale, all three of the schemes produce too much light rain and not enough instances of no rain, such behaviour being in fact much less pronounced for the PC scheme than for the others.

Figure 17 shows the PDFs from the KF scheme over 32 and 64 km<sup>2</sup>. Interestingly, the issue of too much light rain at the grid scale has become an issue of insufficient cases of very light rain, and too much light to moderate rain at 64 km<sup>2</sup>. We suggest that this provides an indication of a problem with the upscaling of rainfall variability: the rainfall field becomes too smooth too readily.

It must be noted here that alternative methods are possible for setting the values of  $\langle c \rangle$  used for each scheme. We have investigated some other approaches and do find some effects on the values of  $A$  obtained. However, any uncertainties in the choice of  $\langle c \rangle$  have no effect on our general conclusions about the upscaling of rainfall variability, which is much improved with the PC scheme compared to the conventional deterministic schemes. It is also worth noting that the spatial and temporal averaging strategy does not strongly affect values of  $A$  obtained for the PC scheme.

## 5. Discussion

The mass flux formalism for deep convective parametrization is based on representing the collective behaviour of an ensemble of convective clouds, subject to a known large-scale forcing. A conventional deterministic parametrization

assumes that the grid scale of the parent model can be identified with the large scale, whereas the Plant–Craig (PC) scheme makes an explicit distinction between those scales. Natural consequences of that distinction are that convective parametrization should be stochastic, and that the input large-scale state used for closure calculations should be a space–time average over a suitable region. The implications of that first consequence were addressed by Plant and Craig (2008), while implications of the second have been considered here by developing the PC scheme for use in three dimensions. The resulting scheme has been shown to produce mean vertical profiles which agree well with established conventional schemes, and with CRM simulations. The statistics of the PC scheme also agree well with the underlying Cohen–Craig theory (Craig and Cohen, 2006), to a similar extent as their corresponding CRM simulations (Cohen and Craig, 2006). In this way, the PC scheme has been shown to produce the same convective statistics as CRM simulations—a key test for any stochastic scheme. The agreement between PC and theory (and, therefore, CRM) is good for a range of model heights, suggesting that the theory remains applicable away from the cloud base. The agreement is also good for a range of model grid lengths, indicating that the PC scheme can adapt correctly within variable-resolution models.

We have investigated what averaging length and time scales are required to produce an input state with which the scheme can yield the correct statistics. An averaging length of 160 km and time of 50 minutes were found to be sufficient for the  $\bar{T}_0 = 8$  K per day experiments. Given that these experiments typically included 307 clouds, on average, over the 512 km square domain, and with a cloud lifetime of 45 minutes, this corresponds to a requirement of roughly 33 clouds (full lifetime equivalent) in the area being averaged.

This requirement can be used to produce a dynamical averaging strategy for operational use of the PC scheme. Of course, the averaging length and time scales vary depending on weather regime, and so the fundamental requirement, at each time step and in each grid box, would be to ensure that a large enough area is taken to include 33 clouds (full lifetime equivalent), based on an estimate of the number of clouds in the grid box in question (obtained, for example, by taking the averaged value from the previous time step).

However, although the spatial averaging is clearly beneficial, there is certainly scope for using less averaging without greatly degrading the statistics. Indeed, a full range of averaging strategies is available from—at one end—the ideal target of 33 clouds (full lifetime equivalent) to—at the other end—the possibility of foregoing the averaging completely if this is necessary due to operational constraints. Although the temporal averaging yields no significant benefit in this paper, it is less computationally intensive than the spatial averaging, and does not require communication between processors in a parallel environment. Given that it does not degrade the performance of the scheme in the current simulations, and that it may yield benefit in other situations, it is suggested here that temporal averaging may still be used as an alternative, or a complement, to spatial averaging if the aforementioned constraints render the spatial averaging unwieldy.

The scheme has been shown to yield the correct scaling for the variability of rainfall rate, across a range of scales. Even for such a simple model set-up, the established conventional schemes do not do this correctly. The improvement of the

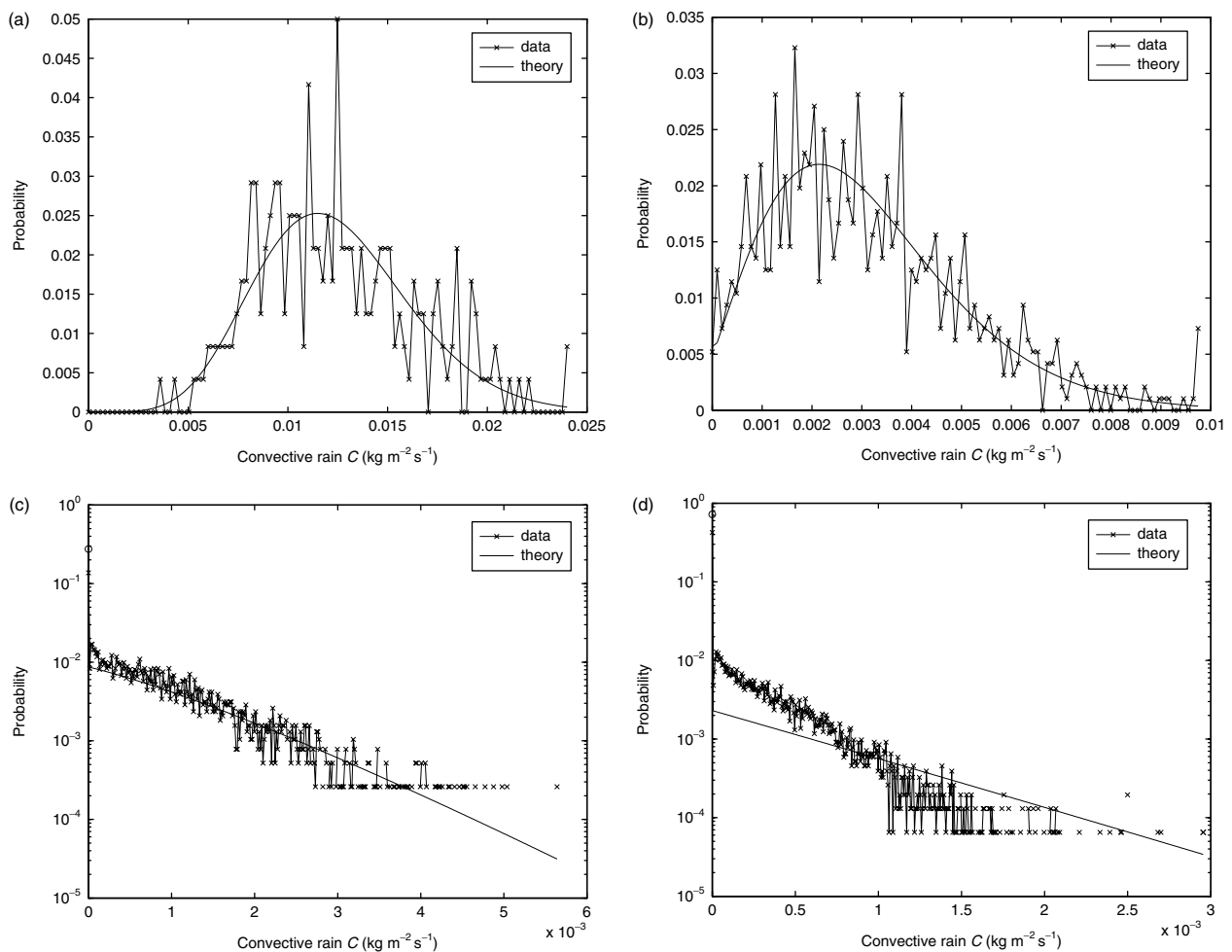


**Figure 16.** PDF for the total convective rainfall  $C$  over horizontal areas of 256 km<sup>2</sup> (a), 128 km<sup>2</sup> (b), 64 km<sup>2</sup> (c) and 32 km<sup>2</sup> (d). The crosses show results from a simulation with the PC scheme for a grid length of 32 km, a cooling rate of  $\dot{T}_0 = 8$  K per day and standard averaging for the input to the scheme. Also shown are the theoretical predictions (solid line) given by Eq. (9). For the two lower scales, the  $y$ -axis is logarithmic, and the circle denotes the value of  $p(0)dC$ .

**Table III.** Measure  $A$  of difference between theoretical and experimental rainfall distributions using three different convection schemes, and computed for four different areas.

Scheme	$\langle c \rangle$ (kg m <sup>-2</sup> s <sup>-1</sup> )	256	128	64	32
PC	$6.0 \times 10^{-4}$	0.369	0.258	0.397	0.684
KF	$5.0 \times 10^{-4}$	0.402	0.283	0.658	1.250
GR	$2.8 \times 10^{-3}$	0.443	0.585	1.259	1.197

The top row lists the length (km) of the side of the accumulation area. In each case the model grid length was 32 km and the cooling rate was  $\dot{T}_0 = 8$  K per day.

scaling produced by the PC scheme, over that produced by conventional schemes, indicates that the stochastic character of the PC scheme captures physically realistic convective variability that will provide a worthwhile improvement to NWP and GCMs.

Work is underway on investigating the impact of the PC scheme on mesoscale NWP forecasts. Groenemeijer and Craig (2011) have shown that the scheme yields significant amounts of variability, as compared to those amounts yielded by perturbations in the initial and boundary conditions, and have investigated how this partition between ‘internal’ and ‘external’ variability changes for different weather regimes, within an ensemble forecast. Additionally,

we are currently conducting a study into the impact on ensemble verification scores, when the conventional convection scheme in the UM is replaced by the PC scheme.

### Acknowledgements

This research was supported by NERC grant NE/D011493/1. Computing support was provided by the NCAS Computer Modelling Service. The authors would also like to thank the following for useful discussions during the course of the project: W. J. Tennant, N. E. Bowler, R. N. Swinbank, S. E. Beare and other staff at the Met Office; and P. H. Groenemeijer and G. C. Craig from DLR/LMU, Munich.

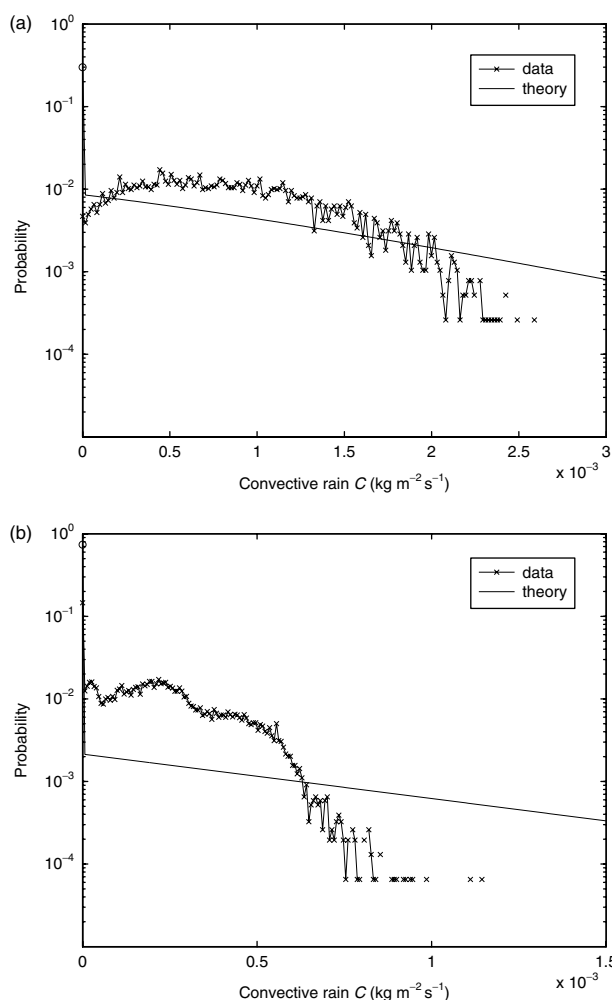


**Figure 17.** PDF for the total convective rainfall  $C$  over horizontal areas of  $64 \text{ km}^2$  (a) and  $32 \text{ km}^2$  (b). The crosses show results from a simulation with the KF scheme for a grid length of  $32 \text{ km}$  and a forcing of  $\bar{T}_0 = 8 \text{ K}$  per day. Also shown are the theoretical predictions (solid line) given by Eq. (9). The circle in each plot denotes the value of  $p(0)dC$ .

## References

- Ball MA, Plant RS. 2008. Comparison of stochastic parameterization approaches in a single-column model. *Phil. Trans. Roy. Soc. A* **366**: 2605–2623.
- Bechtold P, Köhler M, Jung T, Doblas-Reyes F, Leutbecher M, Rodwell MJ, Vitart F, Balsamo G. 2008. Advances in simulating atmospheric variability with the ECMWF model: from synoptic to decadal timescales. *Q. J. R. Meteorol. Soc.* **134**: 1337–1351.
- Bowler NE, Arribas A, Mylne KR, Robertson KB, Beare SE. 2008. The MOGREPS short-range ensemble prediction system. *Q. J. R. Meteorol. Soc.* **134**: 703–722.
- Bright DR, Mullen SL. 2002. Short-range ensemble forecasts of precipitation during the southwest monsoon. *Weather Forecast.* **17**: 1080–1100.
- Buizza R. 1997. Potential forecast skill of ensemble prediction and spread and skill distributions of the ECMWF ensemble prediction system. *Mon. Weather Rev.* **125**: 99–119.
- Buizza R, Miller M, Palmer TN. 1999. Stochastic representation of model uncertainties in the ECMWF Ensemble Prediction System. *Q. J. R. Meteorol. Soc.* **125**: 2887–2908.
- Buizza R, Houtekamer PL, Toth Z, Pellerin G, Wei M, Zhu Y. 2005. A comparison of the ECMWF, MSC, and NCEP global ensemble prediction systems. *Mon. Weather Rev.* **133**: 1076–1097.
- Cohen BG. 2001. 'Fluctuations in an ensemble of cumulus clouds'. PhD thesis, University of Reading, UK.
- Cohen BG, Craig GC. 2006. Fluctuations in an equilibrium convective ensemble. Part II: Numerical experiments. *J. Atmos. Sci.* **63**: 2005–2015.

- Craig GC, Cohen BG. 2006. Fluctuations in an equilibrium convective ensemble. Part I: Theoretical formulation. *J. Atmos. Sci.* **63**: 1996–2004.
- Davies L. 2008. 'Self-organization of convection as a mechanism for memory'. PhD thesis, University of Reading, UK.
- Davies T, Cullen MJP, Malcolm AJ, Mawson MH, Staniforth A, White AA, Wood N. 2005. A new dynamical core for the Met Office's global and regional modelling of the atmosphere. *Q. J. R. Meteorol. Soc.* **131**: 1759–1782.
- Davoudi J, McFarlane NA, Birner T. 2010. Fluctuation of mass flux in a cloud-resolving simulation with interactive radiation. *J. Atmos. Sci.* **67**: 400–418.
- Emanuel KA. 2000. Quasi-equilibrium thinking. In: *General Circulation Model Development*, Randall DA (ed.). Elsevier: Amsterdam; 225–255.
- Gregory D, Rowntree PR. 1990. A mass flux convection scheme with representation of cloud ensemble characteristics and stability-dependent closure. *Mon. Weather Rev.* **118**: 1483–1506.
- Groenemeijer PH, Craig GC. 2011. Ensemble forecasting with a stochastic convective parametrization based on equilibrium statistics. *Atmos. Phys. Chem. Disc.* **11**: 30457–30485, DOI: 10.5194/acpd-11-30457-2011.
- Held IM, Zhao M. 2008. Horizontally homogeneous rotating radiative–convective equilibria at GCM resolution. *J. Atmos. Sci.* **65**: 2003–2013.
- Held IM, Zhao M, Wyman B. 2007. Dynamic radiative–convective equilibria using GCM column physics. *J. Atmos. Sci.* **64**: 228–238.
- Holloway CE, Neelin JD. 2010. Temporal relations of column water vapor and tropical precipitation. *J. Atmos. Sci.* **67**: 1091–1105.
- Jones TR, Randall DA. 2011. Quantifying the limits of convective parameterizations. *J. Geophys. Res.* **116**: D08210, DOI: 10.1029/2010JD014913.
- Kain JS. 2004. The Kain–Fritsch convective parameterization: an update. *J. Appl. Meteorol.* **43**: 170–181.
- Kain JS, Fritsch JM. 1990. A one-dimensional entraining/detraining plume model and its application in convective parameterization. *J. Atmos. Sci.* **47**: 2784–2802.
- Kuo YH, Bresch JF, Cheng MD, Kain J, Parsons DB, Tao WK, Zhang DL. 1997. Summary of a mini workshop on cumulus parameterization for mesoscale models. *Bull. Am. Meteorol. Soc.* **78**: 475–491.
- Lander J, Hoskins BJ. 1997. Believable scales and parameterizations in a spectral transform model. *Mon. Weather Rev.* **125**: 292–303.
- Larson K, Hartmann DL. 2003. Interactions among cloud, water vapor, radiation and large-scale circulation in the tropical climate. Part I: Sensitivity to uniform sea surface temperature changes. *J. Climate* **16**: 1425–1440.
- LeMone MA, Zipser EJ. 1980. Cumulonimbus vertical velocity events in GATE. Part II: Synthesis and model core structure. *J. Atmos. Sci.* **37**: 2458–2469.
- Lin JWB, Neelin JD. 2003. Toward stochastic deep convective parameterization in general circulation models. *Geophys. Res. Lett.* **30**: 1162, DOI: 10.1029/2002GL016203.
- Lock AP, Brown AR, Bush MR, Martin GM, Smith RNB. 2000. A new boundary layer mixing scheme. Part I: Scheme description and single-column model tests. *Mon. Weather Rev.* **128**: 3187–3199.
- Lucas C, Zipser EJ, LeMone MA. 1994. Vertical velocity in oceanic convection off tropical Australia. *J. Atmos. Sci.* **51**: 3183–3193.
- Martin GM, Ringer MA, Pope VD, Jones A, Dearden C, Hinton TJ. 2006. The physical properties of the atmosphere in the new Hadley centre global environmental model (HadGEM1). Part I: Model description and global climatology. *J. Climate* **19**: 1274–1301.
- May PT, Rajopadhyaya DK. 1999. Vertical velocity characteristics of deep convection over Darwin, Australia. *Mon. Weather Rev.* **127**: 1056–1071.
- Moron V, Robertson AW, Ward MN, Camberlin P. 2007. Spatial coherence of tropical rainfall at the regional scale. *J. Climate* **20**: 5244–5263.
- Parodi A, Emanuel K. 2009. A theory for buoyancy and velocity scales in deep moist convection. *J. Atmos. Sci.* **66**: 3449–3463.
- Paulius O, Garner S. 2006. Sensitivity of radiative–convective equilibrium simulations to horizontal resolution. *J. Atmos. Sci.* **63**: 1910–1923.
- Plant RS. 2010. A review of the theoretical basis for bulk mass flux convective parameterization. *Atmos. Chem. Phys.* **10**: 3529–3544.
- Plant RS, Craig GC. 2008. A stochastic parameterization for deep convection based on equilibrium statistics. *J. Atmos. Sci.* **65**: 87–105.
- Ricciardulli L, Sardeshmukh PD. 2002. Local time- and space scales of organized tropical deep convection. *J. Climate* **15**: 2775–2790.
- Robe FR, Emanuel KA. 1996. Moist convective scaling: some inferences from three-dimensional cloud ensemble simulations. *J. Atmos. Sci.* **53**: 3265–3275.



- Shutts G. 2005. A kinetic energy backscatter algorithm for use in ensemble prediction systems. *Q. J. R. Meteorol. Soc.* **131**: 3079–3102.
- Shutts GJ, Gray MEB. 1999. Numerical simulations of convective equilibrium under prescribed forcing. *Q. J. R. Meteorol. Soc.* **125**: 2767–2787.
- Shutts GJ, Palmer TN. 2007. Convective forcing fluctuations in a cloud-resolving model: relevance to the stochastic parameterization problem. *J. Climate* **20**: 187–202.
- Smith DF, Gasiewski AJ, Jackson DL, Wick GA. 2005. Spatial scales of tropical precipitation inferred from TRMM microwave imager data. *IEEE Trans. Geophys. Remote Sens.* **43**: 1542–1551.
- Stiller O. 2009. Efficient moist physics schemes for data assimilation. II: Deep convection. *Q. J. R. Meteorol. Soc.* **135**: 721–738.
- Willett MR, Milton SF. 2006. 'The tropical behaviour of the convective parameterization in aquaplanet simulations and the sensitivity to timestep'. *Forecasting Research Technical Report 482*, Met Office: Exeter, UK.
- Williams PD, Palmer TN (eds). 2009. *Stochastic Physics and Climate Modelling*. Cambridge University Press: Cambridge, UK.
- Wilson DR, Ballard SP. 1999. A microphysically based precipitation scheme for the UK Meteorological Office Unified Model. *Q. J. R. Meteorol. Soc.* **125**: 1607–1636.
- Xu KM, Arakawa A, Krueger SK. 1992. The macroscopic behavior of cumulus ensembles simulated by a cumulus ensemble model. *J. Atmos. Sci.* **49**: 2402–2420.
- Zhang F, Snyder C, Rotunno R. 2003. Effects of moist convection on mesoscale predictability. *J. Atmos. Sci.* **60**: 1173–1185.
- Zhang GJ, McFarlane NA. 1995. Sensitivity of climate simulations to the parameterization of cumulus convection in the Canadian climate centre general circulation model. *Atmosphere–Ocean* **33**: 407–446.